Infrared Thermal Mapping, Analysis and Interpretation in Biomedicine

SELVAN, Arul <http://orcid.org/0000-0001-9222-5538> and CHILDS, Charmaine <http://orcid.org/0000-0002-1558-5633>

Citation:

Copyright and re-use policy

Infrared Thermal Mapping, Analysis and Interpretation in Biomedicine

Arul N. Selvan and Charmaine Childs

Abstract Measurement of body temperature is one of the cornerstones of clinical assessment in medicine. Skin, the largest organ of the human body, is essentially a temperature *mosaic* determined by the rate of blood flow through arterioles and capillaries adjacent to the skin. This makes the conventional methods of 'spot' measurement rather limited in providing detailed information of regional skin temperature. Infrared (IR) thermal imaging however has the potential to provide a robust method of surface temperature mapping in disease states where pathology disturbs the 'normal' distribution of blood flow to skin. To advance image interpretation from the conventional qualitative narrative to a quantitative and robust system, analytical developments focus on digital images and require computer-aided systems to produce results rapidly and safely. Hierarchical clustering-based segmentation (HCS) provides a generic solution to the complex interpretation of thermal data (pixel by pixel) to produce clusters and boundary regions at levels not discernible by human visual processing. In this chapter, HCS has been used to aid the interpretation of wound images and to identify variations in temperature clusters around and along the surgical wound for their clinical relevance in wound infection.

Keywords Infrared · Temperature · Thermal mapping · Wound infection · Image analysis · Hierarchical Clustering-based Segmentation (HCS) · Isotherm · Boundary outlining

A.N. Selvan
Materials and Engineering Research Institute, Sheffield Hallam University, Howards Street, Sheffield S1 1WB, City Campus, UK

C. Childs (✉)
Centre for Health and Social Care Research, Sheffield Hallam University, Montgomery House, Collegiate Campus, Sheffield S10 2BP, UK
e-mail: c.childs@shu.ac.uk
URL: http://www.shu.ac.uk

1 Human Temperature Measurement

Measurement of the temperature of the tissues of the human body is probably one of the most well recognised clinical activities in modern medicine. A change in body temperature, notably fever, has long been regarded as a classical sign of inflammation and infection in man which for centuries was measured with a variety of instruments. In recent years, clinical thermometry has undergone an evolution with a variety of "*liquid in glass, liquid crystal and electronic*" '*thermometers*' in everyday use. The sites for measurement are limited and, by convention, confined to body cavities (mouth, oesophagus, rectum) skin folds and crevices of the groin and axilla (armpit) [21].

However, over the last few decades, advances in thermometry and accompanying technology has evolved such that we are now able to implant temperature sensors deep inside the human body, previously possible only in the experimental laboratory. In the brain for example, being able to implant sensors into injured white matter and/or cerebral ventricles [9] has shown variations in organ temperature from deep to superficial structures [14] and across the brain [8] and has revolutionised our understanding of the pathophysiology of brain damage [27, 36]. Similar variations in regional tissue temperature have also been reported, with non-invasive imaging of healthy brain using ^{1}H magnetic resonance spectroscopy (^{1}HMRS) and imaging (^{1}H MRSI) [7]. That said, we have to recognise the limitations of in situ sensor technology for whole organ temperature measurement. Since the insertion of multiple probes and sensors are not feasible in the clinical setting, the measurement site is generally restricted to just a single '*spot*'. The same is true for skin temperature measurement. When it comes to surface temperature, the skin has long been regarded as a thermal '*mosaic*' [17]. With the knowledge that skin temperature can vary widely across the body, what value might there be in a single skin measurement? More useful would be skin temperature "*mapping*" in body regions where disease manifests upon the skin. Infrared (IR) thermometry provides a solution to both temperature measurement and regional temperature mapping and can be undertaken rapidly and relatively simply.

Non-ionising IR thermal imaging has many advantages. Although not used routinely as a diagnostic clinical tool, it does have potential as a future imaging modality provided that image analysis can be developed to provide reliable routes to interpretation, assessment and diagnosis in medicine. In this chapter, methods for the interpretation of digital thermal imaging in biomedical applications are presented.

2 Infrared Thermal Imaging in Medicine

The use of infrared thermal imaging in health care is not a recent phenomenon. Thermography in breast cancer screening began in 1956 when Lawson [19] observed that skin temperature overlying a breast tumour was higher than that of

'*normal*' skin. However, using thermography without a standardised protocol for imaging, patient preparation, control of ambient temperature or physician training led to scepticism; the technique not being perceived well for "*diagnostic/screening*" accuracy. It subsequently suffered a demise [42]. Alternative imaging modalities at this time; X-ray, proton magnetic resonance imaging ([1]HMRI) computed tomography (CT) whilst costly had a superior reputation for reliability and clinical utility. However, it is now recognised that when used repeatedly in diagnostics, all incur a degree of hazard to health due to ionising radiation load; particularly for neonates and young children [22, 26]. By contrast, IR thermography does not penetrate structures below the skin and is non-ionising.

The utility of IR thermal imaging is underpinned by its penetration depth. IR radiation is not emitted by skin at depths greater than 5.0 mm [20] thus it is unable to "*image*" deep tissue and organs. That said, many physiological and pathophysiological changes "*trigger*" alterations in skin dermis via capillary networks, particularly in acral regions (toe, finger, ear, tip of nose). Such changes occur either intrinsically through local biochemical stimuli, and/or by external factors (heat/cold for example) via vascular, neurological and/or neurovascular pathways [20]. This makes IR imaging at the surface of real value for a number of prognostic and diagnostic capabilities where changes in skin blood flow, and thus skin temperature, provide clinically relevant information. The significant advances in IR detectors and technology, along with improvements in the development of image processing techniques have, over the last 5 years, seen a re-emergence of interest in IR imaging with a successful reported use in oncology, pain management, vascular disorders, arthritis/rheumatism, neurology, sports and rehabilitation medicine [11].

# 3 Digital Medical Thermal Imaging Interpretation

Typically, thermal images are inspected and interpreted using the following methods:

- Qualitative or a narrative report determined by visually inspecting the image to identify differences in the colour map corresponding to temperature (°C/°F) (Fig. 1a).
- Quantitative analysis of a region of interest (ROI) or "*spot*" (pixel) measures (Fig. 1b) with options for including average, maximum and minimum values within a ROI.
- Image analysis, in its most simple form, relies solely on the variation in colour of the thermogram which corresponds to a temperature range [39].

3.1 Issues Associated with Visual Inspection of Thermal Images

Until recently, IR thermal cameras were constructed with sensors having low resolution only (e.g. 160 × 120 pixels) but, with advances in detector technology,

Fig. 1 Temperature values in a thermal image displayed using different colour palettes (**a**, **b**). The locations of interest *Sp1* and *Sp2* are better differentiated visually when the temperature values are displayed using colour palette (**b**) versus (**a**) and reveals the potential impact of colour palette choice for interpretation. To choose the right colour palette the user may need to know what they would like to highlight by differentiating from the surrounding area. For example in this case, the pain site (approximate location provided by the patient)
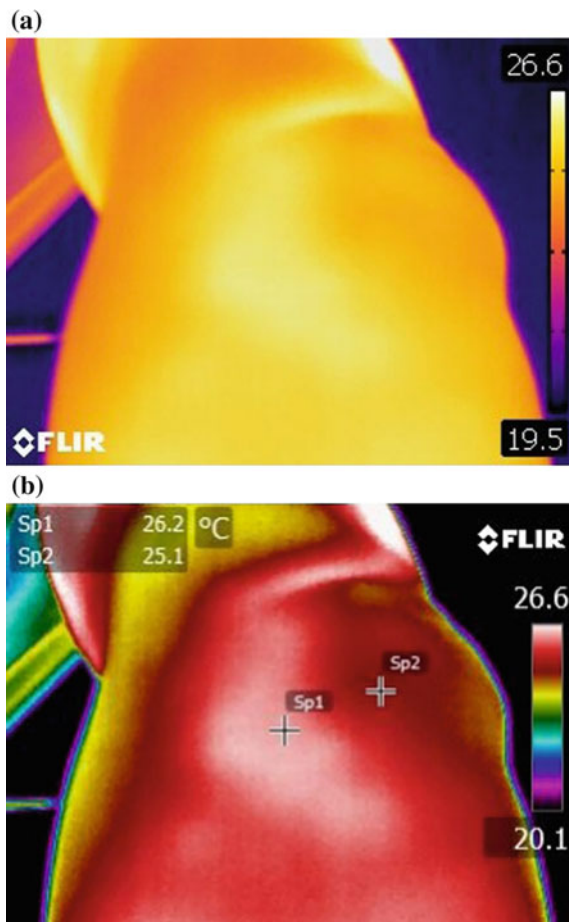
improved thermal sensitivity with possible pixel resolution of (640×480–1024×768) are available as affordable thermal imaging systems. The problem is that human visual processing is not capable of perceiving all of the subtle information present in such high resolution images. Thermal pattern-recognition computer software systems are therefore required to "*extract*" information of thermal values "*hidden*" within the data provided by the thermal camera manufacturers' dedicated software. For example in Fig. 1a, the skin surface temperature over this anatomical region appears relatively homogeneous in colour. However, post-processing with camera software identifies two distinct regions which differ by approximately 1 °C when using measurement spots to provide temperature values at each selected pixel location (SP1 and SP2) and referenced with the temperature key (Fig. 1b). This simple image analysis can be advanced further but requires far greater systems complexity to identify temperature variations over very small areas; for example, between groups of pixels. A system for defining (pixel) areas of
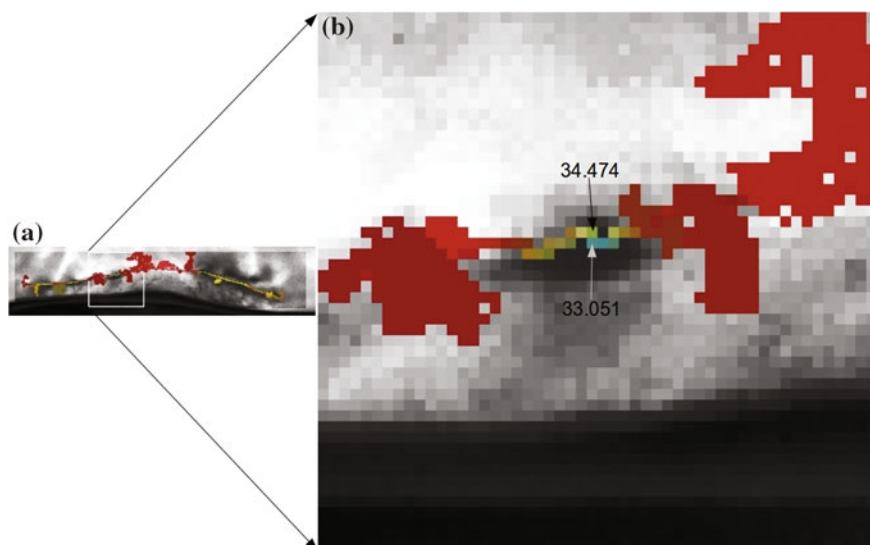
Fig. 2 A typical thermal image where there is a temperature variation of almost 1.5 °C across a single pixel distance. These locations might be missed on casual visual inspection and may need software tools to highlight the dissimilarity

similarity may then be required. As an example, Fig. 2 shows temperature variation of approximately 1.5 °C across single pixel locations. This temperature variation could be lost or overlooked on visual inspection but may be identified easily with a computer-aided pixel highlighting process.

In medicine, clues to the identification of skin/body regions where disease or injury may exist can be provided by the patient him/herself. In Fig. 3a, the patient had complained of pain at the muscles of the thenar eminence. In Fig. 3a, the painful region is identified by an arrow. An adjacent spot measure (SP2) reveals the temperature value; one of a number of regions in this thermogram close to the maximum value in the field of view (maximum being 34.4 °C). In Fig. 3b much greater detail is provided by exploring pixel boundaries around the site (arrow). At least three different colour coded regions can be identified within which the temperature values are similar. By using computer-aided software, it is possible to distinguish each of these regions as a separate temperature "*boundary*". Furthermore, the boundaries make the size and shape of each region, having similar temperature values, become evident. In this way, these images have the potential to map areas of skin temperature linked to the anatomical distribution of pain. This method for outlining areas of similar temperature will aid the objective assessment of the size and position of the area of interest because accuracy of diagnosis depends on how well the segmentation of the ROI is performed in a thermogram [18].

Comparing the ROI from images in Fig. 4a, b, it can be seen how the loss of visual detail inherent in human visual perception can be overcome by further
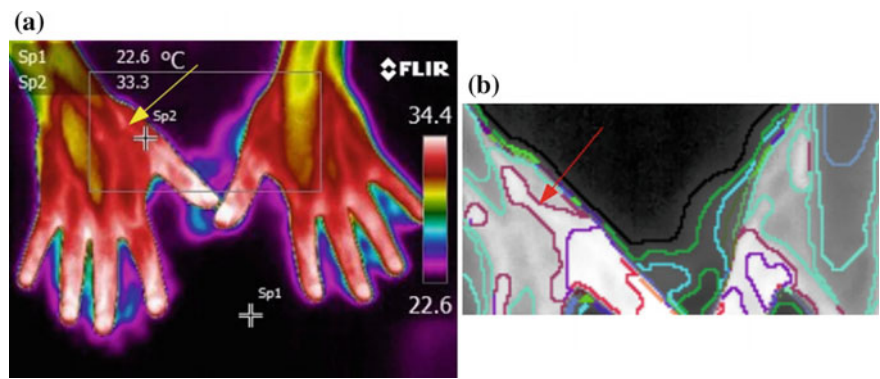
Fig. 3 Hand thermal image showing location of patient-reported pain thought due to underlying inflammation (*yellow arrow*). In **a,** pixel spot (*Sp2*) indicates the pixel temperature at adjacent skin site to the painful area. Computer-aided software tools system applied to (**a**) defines the areas of similar temperature and noting the extent and pattern of the temperature region commensurate with the painful area (*red arrow*) (**b**)
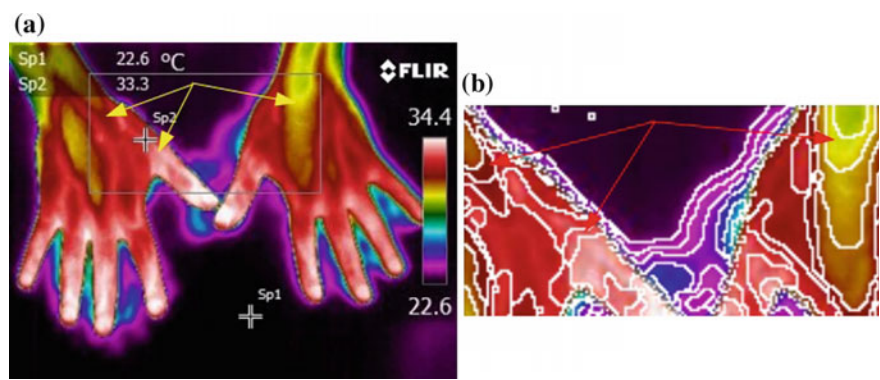

Fig. 4 Isotherms plotted by a computer programme aids visualisation of fine gradations of temperature in the region (defined by the "box") in (**a**). For example, around the locations identified at the (*yellow arrows*) (**a**) the fine gradations of temperature changes are highlighted by using isotherms (*Red arrows*) (**b**)

discrimination of pixels and boundary patterns achieved by the use of isotherms. In this context, isotherms are curves which enclose regions of similar temperature patterns. The isothermal patterns of Fig. 4b show greater detail than information in Fig. 4a and have been produced by a boundary outlining software [29] to enhance image information and to reveal the size and shape of regions with the same (and different) temperature characteristics. By using isothermal patterns and boundary regions, fine resolution and greater information from the same original image can be obtained. Thus, computer generated boundaries aid the visualisation of fine gradations of temperature changes within an area having a seemingly uniform temperature.

Given the potential for computer-aided image analysis to reveal details of the user-drawn ROI (not possible on visual inspection using the software provided by proprietary systems), there is an emerging interest in the development of 'smart' image processing algorithms to enhance the interpretation and analysis of thermal signatures.

We have previously reported the variation in temperature along two different surgical wound types; wounds produced after closure of enterostoma [34] and after caesarean section [10]. We piloted the use of an image processing algorithm; Hierarchical Clustering-based Segmentation (HCS) [29], in detecting anomalies in temperature along the scar [10].

4 Computer-Assisted Medical Thermal Image Interpretation

Anomaly detection in infrared (IR) images is a challenging task. Frize et al. [15] have identified a number of factors which can confound the accuracy of the temperature values acquired, including emissivity, external conditions (temperature, humidity) and imaging surface factors (material, surface properties, orientation) all of which produce IR images of low signal-to-noise ratio [4]. This introduces inaccuracy in obtaining the actual temperature values and contributes to measurement uncertainty.

The most important step in developing a computer-assisted anomaly detection system and application for analysis of thermal images is to segment relevant thermal information from thermal noise. Numerous algorithms are available in the literature for detecting boundaries to segment ROI in visible and optical images. However, because of the non-uniformity of IR images, revealed by varied pixel values representing similar temperature across the image [6], boundary regions in thermal images are not defined clearly. Software techniques used successfully in detecting boundaries in optical (visible) images have the drawback of being unable to form continuous, distinct and meaningful boundaries around an ROI in thermograms; they are therefore unreliable for segmenting IR images [44].

Designs for computer-assisted methods for the interpretation of thermal images are available, for example, to assist the user in objective identification of skin 'hot' spots. Snekhalatha et al. [35] implemented an automated thermal image segmentation of a hot spot region of the hand. Similarly, because a regular ROI such as a rectangle, square, circle or elipse, poorly outlines certain anatomical regions [13]. Vardasca et al. [40] designed an automated ROI fitting method to address the issues associated with obtaining a representative temperature value from a user-drawn regular ROI from thermal images of limbs. These examples suggest that automation of thermal images are typically for "bespoke" applications.

In this chapter, we discuss the development of a generic thermal image segmentation process to extract thermal features considered to be '*abnormal*' and using a Hierarchical Clustering-based Segmentation (HCS) design and process [29]. HCS segments an image as a set of regions with each region composed of sub-regions and which are, themselves, composed of sub-regions, and so on [16]. In this way, HCS is a dissimilarity highlighting process that yields a hierarchy of segmentation results. It is well suited to address the issues associated with the segmentation of 'noisy' thermal image data.

In separating out the ROI, *thresholding* is used. The separation is based on the variation of pixel values between the regions' pixels and the surrounding pixels. For example in a grey scale image with pixel values ranging from zero to 255, the variation of (difference in) pixel values between parts (regions) can be between zero and 255. In the thresholding process, a part of the image is segmented as a separate region if its pixel values vary from the surrounding pixel values by a threshold value (T). For a low threshold value, pixels having even the smallest difference from the surrounding pixel values will be *segmented* as a separate region. Thus, a low threshold value will locate boundaries of regions having the most subtle of differences. As these small pixel value differences may be because of the non-uniformity of IR images, the detected boundaries will be spurious [12]. By contrast, higher threshold values will detect only the boundaries of regions where there are major difference with the surroundings but by using a higher threshold, the downside is that there are likely discontinuities in the detected boundaries [12].

Identifying boundaries where only a single threshold value is employed has two problems [1, 2]. First, the most appropriate threshold value will depend greatly on the application, i.e. whether identification is required for major boundaries or subtle boundaries only. Second, and importantly, thresholding using a single threshold will result in loss of useful boundary information, which might otherwise be found for different threshold values.

Unlike other segmentation processes which favour identification of the boundaries between different regions by choosing a (single) threshold value, the HCS process is based on a non-thresholded boundary identifying process. That is, no threshold value is used. However, recognising that the process does, indeed, need some form of "*thresholding*" approach to identify the boundaries of different regions in an image, the HCS process rather than using a single threshold value, instead uses a "*hierarchical*" level of thresholding to identify the boundaries between different regions in the image.

4.1 Design of Hierarchical Clustering-Based Segmentation (HCS) as an Aid to Interpret Medical Thermal Images

The human visual system processes images at varying resolutions; coarse to fine. For example, given an anatomical image of the cross section of a skull, at a coarse level a radiologist can visualise the image as distinct regions belonging to soft

tissues or bone. At a fine level, different types of soft tissues are also identified. At a still finer level and, given the appropriate imaging modality, the radiologist will be able to distinguish "*abnormal*" regions (e.g. commensurate with ischaemia) within the same tissue type. This example illustrates a "*resolution*" hierarchy from coarse (bone) fine (tissue) and still finer (blood within tissue) within an image. Since the early days of computer vision, this hierarchical structure of visual perception has motivated clustering techniques for image segmentation [25]. So in a computer model representation, the segmentation process is modelled as a process of grouping visual information, where the details are grouped into objects, and objects into classes of objects. Thus, starting from the composite segmentation, the perceptual organization of the image can be represented by a tree of regions, ordered by inclusion. The root of the tree is the entire scene, the leaves are the finest details and each region represents an object at a certain scale of observation [1].

Hierarchical Clustering-based Segmentation (HCS) [28–30] implements the traditional agglomerative clustering [23] where the regions of an initial partition are iteratively merged and automatically generate a hierarchy of segmented images (Fig. 5); for example, Fig. 6 (top row of images; left to right).

The hierarchy of segmented images is generated by partitioning an image into its constituent regions at hierarchical levels of "*allowable dissimilarity*" (threshold value) between its different regions. At any particular level in the hierarchy, the segmentation process will cluster together all the pixels and/or regions which have dissimilarity value among them; less than or equal to the dissimilarity allowed for that level (Fig. 5).
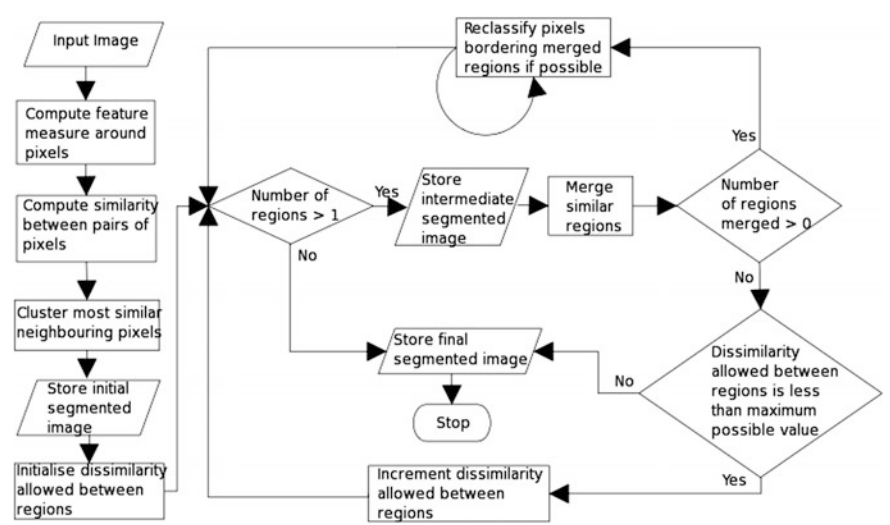

Fig. 5 Flow chart illustrating the working of the HCS process. The input image is initially segmented into regions by clustering similar neighbouring pixels. The initial segmentation of the region is merged for different *allowable dissimilarities*, between regions, yielding a hierarchy of segmented images. Reproduced from [28]
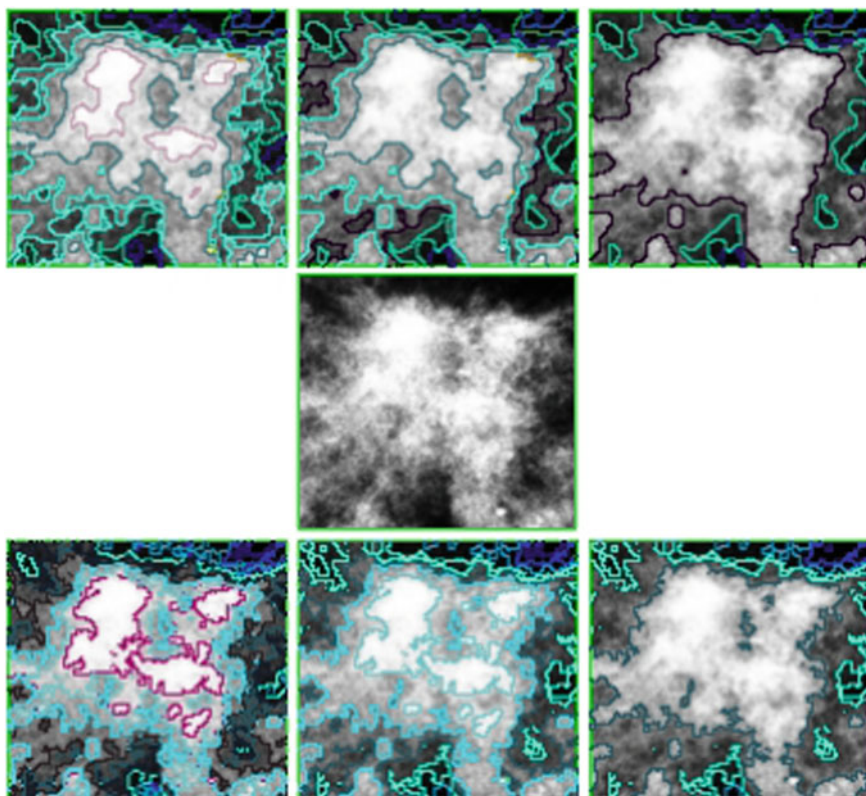
Fig. 6 Comparison of segmentation output of an ill-defined "*abnormality*" from an X-ray mammogram image (*middle row*) **with** border-pixel-re-classification (*top row*) and **without** border-pixel-re-classification(*bottom row*). The delineated cluster boundaries with border-pixel-re-classification (*top row*) are more easily visualised as distinct visual clusters when compared to the cluster boundaries delineated without border-pixel-re-classification (*bottom row*) and is an example of HCS process' capability

A unique feature of the HCS process is the border pixel classification operation (flow-chart Fig. 5). Border pixel reclassification is considered only for those pixels on the boundary of the clusters which had been merged with other clusters. These boundary pixels are removed one at a time from their original clusters. The pixel removed is considered as a region of its own and the similarity between the one pixel region and the regions bordering it (which include the original cluster to which it belonged) are found and the single pixel region merged with the most similar bordering region. Border pixel reclassification aides in over-riding local inhomogeneity while clustering similar pixels/regions.

An example of HCS border pixel re-classification in use can be demonstrated by the visually smooth border delineation obtained in Fig. 6. The central image (middle row) is the image of an abnormality having ill-defined boundaries presented in an

X-ray mammogram. It can be seen from the border outlined images that the HCS process (with border pixel reclassification—top row) achieves far better results in delineating the different regions within the abnormality when compared to the segmentation without border-pixel-re-classification (bottom row). The border pixel re-classification operation of the HCS process generates visually smooth boundaries and also identifies more appropriate boundaries when compared to other similar segmentation processes such as Tilton's [37] Hierarchical Segmentation (HSEG) [38]. For further details with relevant example see Selvan [29].

Since the HCS process is a generic segmentation process, it is applicable and equally successful at segmentation and outlining boundaries of ROI in digital images from any source whether from X-ray or thermal image. This makes HCS a versatile process which has been demonstrated successfully and without any modifications (e.g. parameter tuning) to segment images of the natural environment (e.g. birds, trees) [29] and diagnostic images obtained using different modalities; ultrasound images [28], CT [31], X-ray mammograms [32], magnetic resonance imaging [33] and digital medical thermal image (DMTI) [10].

5 HCS Process in Thermal Image Analysis of Surgical Wounds

In clinical practice, the assessment of surgical wounds for surgical site infection is largely undertaken using wound scoring tables and criteria (e.g. [5, 41, 43]). There are currently no independent quantitative technologies for wound assessment. Typically, however, descriptive narratives are used to describe the state of a wound and to undertake wound healing assessments [24].

Here we describe a novel method to aid the user to:

- visualise the thermal pattern to report information for a more robust qualitative analysis
- provide quantitative measures for wound analysis.

5.1 HCS Process Aided Evaluation of the Temperature Variation of the Surgical Wound

Previous studies report a relationship between temperature and skin viability during inflammation and infection. For example, raised skin temperature is recognised as a sign of inflammation [5]. By contrast, a fall in skin temperature can occur during vascular insufficiency, ischaemia and necrosis [24]. In surgical wounds, we have recently observed '*cold spots*' in the thermograms of surgical wounds which

subsequently were shown to be infected [34]. More recently, we have designed and used the HCS process-based method to obtain quantitative measures to undertake an objective and independent assessment of healthy and infected surgical wounds [10]. For detailed information of the technique see Childs et al. [10] but a brief description is provided here where the steps involved in the designed HCS process include the following:

(a) HCS processing of a ROI around the wound site. A box shaped ROI around the wound site is chosen by the user (Fig. 7a)
(b) comparison of the wound site with a nearby healthy area.

(a) HCS Processing of a ROI Around the Wound Site The main purpose of this step is to highlight regions of different temperature values in an automated and objective manner. The HCS process is applied within the user outlined ROI (Fig. 7a) around the wound site.

The HCS process generates a hierarchy of segmentation output, for different values of allowable dissimilarity, amongst the pixels collated to form regions of similar temperature profiles. From the hundreds of segmentations, the user may make use only of the relevant segmentations having useful segmentation outputs. Briefly, in this example, the user has chosen four different segmentation outputs ranging from the segmentation having 253 regions to the segmentation having 11 regions only (Fig. 7b).
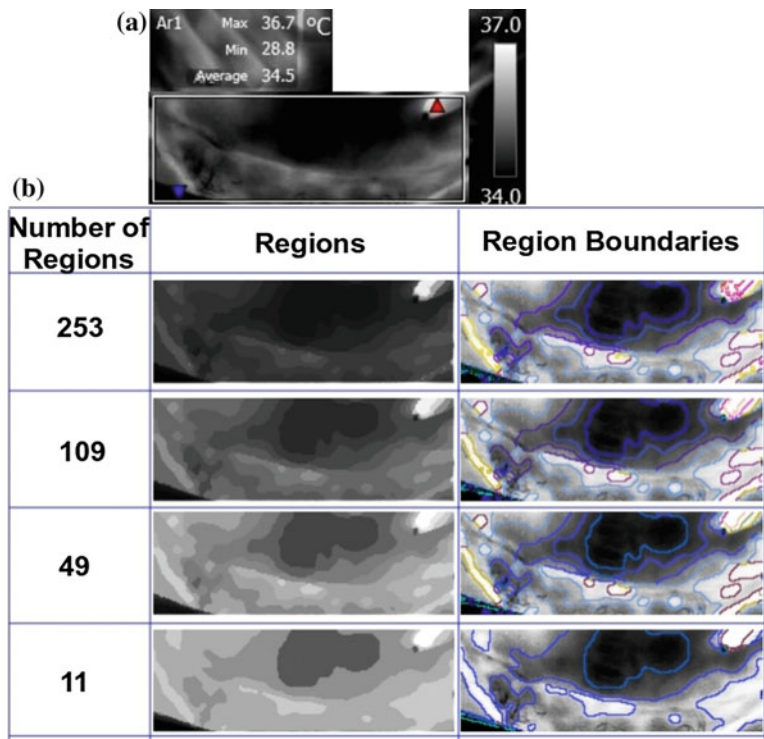
The segmentation having 253 regions will be produced when a low threshold of dissimilarity is allowed between regions. Hence a lesser number of regions will be merged. The segmentation with 11 regions will be produced when a higher value for the dissimilarity threshold is allowed for merging. This facilitates a higher number of regions to merge. In each of the cases (low or high threshold dissimilarity) the region images were produced by mapping the average temperature value of the pixels contained within a region to 256 grey scale levels. The boundary images were produced by plotting the border of the different regions onto the 256 level representations of the radiometric data (Fig. 7a).

From the different segmentation outputs generated, the user may choose segmentation(s) of interest to generate quantitative measures for each of the regions. On inspecting the different segmentations (Fig. 7b), the segmentation with 253 regions was chosen for further analysis and to extract the quantitative (temperature) measurements (Fig. 8). The upper panel shows the locations of interest (locations 1–11) and the corresponding temperature boundary regions (lower panel). In this way, the user can identify the variability in temperature regions across the ROI. In summary, the usefulness of the HCS process in outlining regions of similar temperature profile are as follows:

• The highlighted (boundary outlined) areas will aid the user to visualise, in detail, ROI including the shape and size of "*abnormal*" regions and the variability in temperature within regions which "*at first sight*" appear similar (Fig. 7).

- The process will aid the user to automatically derive quantitative measures of the highlighted (boundary outlined) areas in an objective manner (Fig. 8).

The process can also be used to automatically estimate the summary statistics of the temperature difference between two ROIs; in this example, the regions of the wound and of undamaged skin (Fig. 9c). In this example, marked differences in temperature are evident across the wound and in excess of 1.5 °C.
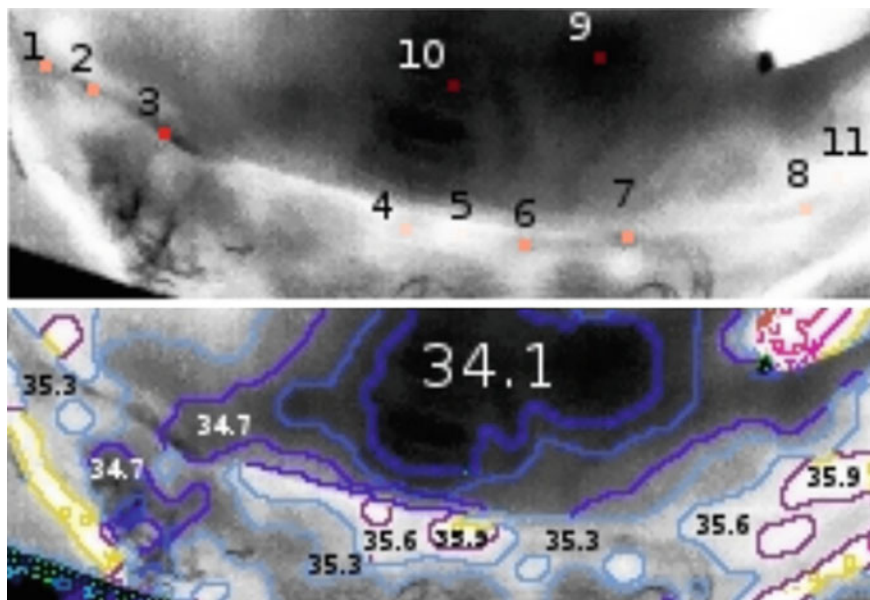

Fig. 7 Thermal image of a surgical wound site in grey scale with user outlined (*white*) box. The ROI is marked around the wound site (**a**). The summary statistics (maximum, minimum, average) of the temperature values within the ROI are estimated by the camera software (**a**); in this example, FLIR systems, Sweden. In (**b**) the region images display the average temperature value within the region mapped to 256 grey levels. The boundaries are marked on the grey shade thermal image (**a**). The HCS process will generate hundreds of segmentation outputs. The regions and boundary images shown in (**b**) are a sample output to illustrate that, when the *allowable dissimilarity value* is increased, the number of regions decrease because more regions will merge. For example when there are 253 regions, the central region (*locations 9, 10 upper panel* Fig. 8) reveals three bounded and segmented regions which range from *34.1 to 34.7 °C*

Fig. 8 HCS process' boundaries aid the user to visualise the different temperature patterns and estimate objective measures; average temperature values of different regions with similar temperature. This is much more appropriate when compared to the summary statistics estimated by the camera software for regular shape ROI (Fig. 7a)

(b) Comparison of the Wound Site with a Nearby Healthy Area Locations of interest along the wound site are noted as are adjacent locations marking healthy areas (Fig. 9a). From the output of the HCS process, regions over the area of healthy skin and the regions over the surgical wound are selected/identified for a user-chosen "*low*" dissimilarity level of 10% (i.e. each segmented region allows inclusion of pixels which differ from each other by not more than 10%) (Fig. 9b). The process automatically estimates the summary statistics of the temperature difference between the regions of the wound and the regions of the healthy area (Fig. 9c). In this example, there are wide variations between wound and adjacent healthy skin. For example, from the summary statistics generated from the HCS process for the image shown in Fig. 9, the wound site was maximally 1.6 °C lower, and maximally 1.2 °C higher, than healthy skin at loci shown (average differences being 0.53° and 0.45°, respectively). In addition, the temperature values along the wound estimated by the HCS process are average (34 °C), lowest (33.8 °C) and highest (35.4 °C) at loci shown in the figure and reveal significant temperature gradients within the ROI of the surgical wound.
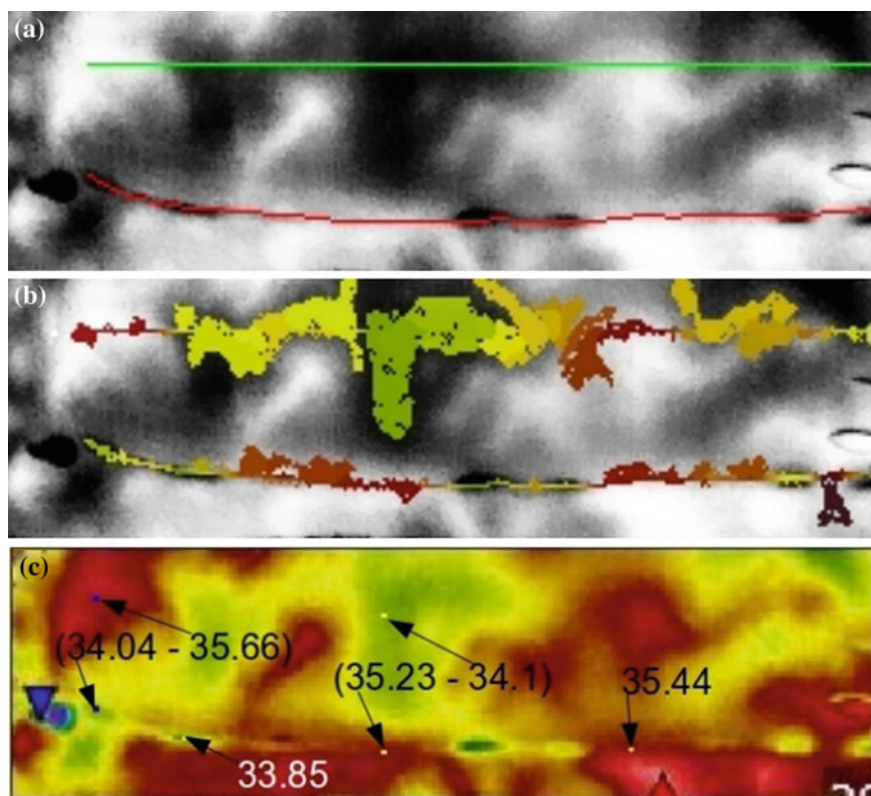
Fig. 9 User tagged locations along the wound (*red curve*) and along a healthy area nearby (*green line*) (**a**). Regions identified by the HCS process containing user tagged locations along the healthy area and along the wound (**b**) at a *dissimilarity level* of 10%. (**c**) Comparisons of temperature values of the regions along the wound and along the healthy area are identified and at three loci differ by 1.2–1.6 °C

6 Summary

Although the temperature of mammalian internal organs are considered relatively uniform (and constant), recent studies have shown that significant temperature gradients do occur [7, 8, 14]; even in a thermally "*shielded*" organ, brain. Whilst temperature shielding, due primarily to the effects of incoming arterial blood [45] would be expected to obviate large temperature gradients within internal structures, this is not the case for skin.

Since the seminal works of Aschoff and Wever in 1968 [3] variability of the body "*shell*" with temperature in excess of 10 °C are not unusual in healthy subjects. Furthermore, a variable counter current heat exchange between arterial and venous blood in limbs and digital extremities (hands, feet) enhances the temperature gradient of the peripheral "*shell*".

By undertaking a comprehensive assessment of healthy and injured skin by IR thermal mapping, combined with a computer-aided system to aid visual processing, we have exploited a variety of well-established image analysis techniques (e.g. hierarchical clustering, isotherm patterning) to produce an objective, robust method to obtain a hierarchy of thermal segments and boundaries to improve upon "*what we see*". Our work has allowed us to "*see more*" of the surgical wound and to set-in-train a quantitative, independent HCS technique of wound imaging systems to explore further the temperature mosaic which exists along the surgical wound for its potential future clinical utility.

References

1. Arbelaez, P.: Boundary extraction in natural images using ultrametric contour maps. In: Proceedings 5th IEEE Workshop on Perceptual Organization in Computer Vision (POCV'06), New York, USA, June 2006 (2006)
2. Arbelaez, P., Fowlkes, C., Martin, D.: The Berkeley segmentation dataset and benchmark June, 2007 (2007). http://www.eecs.berkeley.edu/Research/Projects/CS/vision/bsds/. Accessed 24 June 2016
3. Aschoff, J., Wever, R.: Cited in Stainer MW, Mount LE, Blight J. Energy balance and temperature regulation. Cambridge University Press, 1984 (1958)
4. Bal, A., Alam, A.S.: Automatic target tracking in FLIR image sequences using intensity variation function and template modelling. IEEE Trans. Instrum. Meas. **54**(5), 846–852 (2005)
5. Bharara, M., Schoess, J., Nouvong, A., Armstong, D.G.: Wound inflammatory index: a "proof of concept" study to assess wound healing trajectory. J. Diabet. Sci. Technol. **4**(4), 773–779 (2010)
6. Budzan, S., Wyzgolik, R.: Remarks on noise removal in infrared images. Measur. Autom. Monitor. **61**(06) (2015)
7. Childs, C., Hiltunen, Y., Vidyasagar, R., Kauppinen, R.A.: Determination of regional brain temperature using proton magnetic resonance spectroscopy to access brain-body temperature differences in healthy human subjects. Magn. Reson. Med. **56**, 1–9 (2006)
8. Childs, C., Shen, L.: Regional Pressure and temperature variations across the injured human brain: comparisons between intraparenchymal and ventricular measurements. Crit. Care **19**, 267 (2015). doi:10.1186/s13054-015-0982-x
9. Childs, C., Wang, L., Neoh, B.K., Goh, H.K., Zu, M.M., Aung, P.W., Yeo, T.T.: Multi-parameter brain tissue microsensor and interface systems calibration, reliability and user experiences of pressure and temperature sensors in the setting of neurointensive care. J. Med. Eng. Technol. Early Online, 1–12 (2014). doi:10.3109/03091902.2014.937834
10. Childs, C., Siraj, M.R., Fair, F.J., Selvan, A.N., Soltani, H., Wilmott, J., Farrell, T.: Thermal territories of the abdomen after caesarean section birth: infrared thermography and analysis approaches to surgical site assessment. J. Wound Care **25**(9), 499–512 (2016)

11. Diakides, N.A., Bronzino, J.D. (eds): Medical infrared imaging. CRC Press ISBN 9780849390272 (2008)
12. Dougherty, G.: Digital Image Processing for Medical Applications. Cambridge University Press (2009)
13. Duarte, A., Carrão, L., Espanha, M., Vianad, T., Freitas, D., Bártolod, P., Fariaa, P., Almeidaa, H.A.: Segmentation algorithms for thermal images. Procedia Technol. **16**, 1560–1569 (2014)
14. Fountas, K.N., Kapsalaki, E.Z., Felets, C.H., Smisson III, H.F., Johnston, K.W., Robinson, J. S.: Intracranial temperature: Is it different throughout the brain? Neurocritical Care **4**(2):195–200 (2004)
15. Frize, M., Karsh, J., Herry, C., Adéa, C., Aleem, I., Payeur, P.: Preliminary results of severity of illness measures of rheumatoid arthritis using infrared imaging. In: MeMeA 2009—International Workshop on Medical Measurements and Applications Cetraro, Italy May 29–30, 2009 (2009)
16. Griffin, L.D., Colchester, A.C.F., Roll, S.A., Studholme, C.S.: Hierarchical segmentation satisfying constraints. In: British Machine Vision Conference, UK,1994 (1994)
17. Henane, R., Bittel, J., Bansillon, V.: Partitional calorimetry measurements of energy exchange in severely burned patients. Burns **7**(3), 180–189 (1981)
18. Kapoor, P., Prasad, S.V.A.V., Patni, S.: Image segmentation and asymmetry analysis of breast thermograms for tumor detection. Int. J. Comput. Appl. **50** (2012)
19. Lawson, R.: Implications of surface temperatures in the diagnosis of breast cancer. Can. Med. Assoc. J. **75** (1956)
20. Leando, P.: Digital infrared thermal imaging (DITI) for referring health care practitioners. Meditherm Inc. (2003)
21. Lefrant, J.-Y., Muller, L., Emmanuel Coussaye, J., Benbabaali, M., Lebris, C., Zeitoun, N., Mari, C., Saissi, G., Ripart, J., Eledjam, J.-J.: Temperature measurement in intensive care patients: comparison of urinary bladder, oesophageal, rectal, axillary, and inguinal methods versus pulmonary artery core temperature. Intensiv. Care Med. **29**, 414–418 (2003)
22. Matthews, J.D., Forsythe, A.V., Brady, Z., Butler, M.W., Georgen, S.K., Byrnes, G.B., Giles, G.G., Wallace, A.B., Anderson, P.R., Guiver, T.A., McGale, P., Cain, T.M., Dowty, G.J.G., Bickerstaffe, A.C., Darby, S.C.: Cancer risk in 680,000 people exposed to computed tomography scans in childhood or adolescence: data linkage study of 11 million Australians. BMJ **346**, f2360 (2013)
23. Nadler, M., Smith, E.P.: Pattern Recognition Engineering. Wiley, New York (1993)
24. Nowakowski, A., Kaczmarek, M., Moderhak, M., Siondalski, P.: Thermal imaging in wound healing diagnostics. Measur. Autom. Monitor. **61**(06) (2015)
25. Ohlander, R., Price, K., Reddy, R.: Picture segmentation by a recursive region splitting method. Comput. Graph. Image Process. **8**, 313–333 (1978)
26. Pearce, M.S., Salotti, J.A., Little, M.P., McHugh, K., LeeC, Kim K.P., deGonzalez, A.B., et al.: Radiation exposure form CT scans in childhood and subsequent risk of leukaemia and brain tumours: a retrospective cohort study. Lancet **380**, 499–505 (2012)
27. Sacho, R.S., Childs, C.: The significance of altered temperature after traumatic brain injury: an analysis of investigations in experimental and human studies: Part 2. Br. J. Neurosurg. **22**(4), 497–507 (2008)
28. Selvan, A.N.: Highlighting dissimilarity in medical images using hierarchical clustering-based segmentation (HCS). MPhil. Dissertation, Faculty of Arts Computing Engineering and Sciences, Sheffield Hallam University, Sheffield, UK (2007)
29. Selvan, A.N.: Boundary extraction in images using hierarchical clustering-based segmentation (HCS). In: British Machine Vision Conference (Student workshop) Dundee, UK, Sept 2011 (2011)
30. Selvan, A.N.: Hierarchical clustering-based segmentation (HCS) aided diagnostic image interpretation and monitoring. Doctoral Dissertation, Faculty of Arts Computing Engineering and Sciences, Sheffield Hallam University, Sheffield, UK (2012)

31. Selvan, A.N., Saatchi, R., Ferris, C.M.: Improving medical image perception by hierarchical clustering based segmentation. In: 9th International Conference on Information Technology and Applications in Biomedicine, Larnaka, Cyprus, 4–7 Nov 2009 (2009)
32. Selvan, A.N., Saatchi, R., Ferris, C.M.: Computer aided monitoring of breast abnormalities in X-ray mammograms. In: Medical Image Understanding and Analysis Conference, London, UK (2011)
33. Selvan, A.N., Pettitt, S., Wright, C.: Hierarchical clustering-based segmentation (HCS) aided interpretation of the DCE MR images of the prostate. In: Medical Image Understanding and Analysis Conference, Lincoln, UK, July 2015 (2015)
34. Siah, C.J.R., Childs, C.: Thermographic mapping of the abdomen in healthy subjects and patients after enterostoma. J. Wound Care **24**(3) (2015)
35. Snekhalatha, U., Anburajan, M., Sowmiya, V., Venkatraman, B., Menaka, M.: Automated hand thermal image segmentation and feature extraction in the evaluation of rheumatoid arthritis. Proc. Inst. Mech. Eng. [H] **229**(4), 319–331 (2015)
36. Soukup, J., Rieger, C., Holz, C., Miko, I., Nemeth, N., Menzel, M.: Temperature gradient between brain tissue and arterial bloof mirrors the flow-metabolism relationship in uninjured brain: an experimental study. Acta Anaesthesiol. Scand. **51**, 872–879 (2007)
37. Tilton, J.C.: Hierarchical image segmentation. On-line Journal of Space Communication Issue No. 3 Winter 2003 Research and Applications (2003)
38. Tilton, J.C.: Hierarchical image segmentation (2016). http://science.gsfc.nasa.gov/606.3/TILTON/hseg.html. Accessed 11 Aug 2016
39. Vardasca, R., Bajwa, U.: Segmentation and noise removal on thermographic images of hands. Thermol. Int. **18**(3), 99–104 (2008)
40. Vardasca, R., Gabriel, J., Jones, C.D., Plassmann, P., Ring, E.F.J.: A template based method for normalizing thermal images of the human body. In: The 12th International Conference on Quantitative infrared Thermography, at Bordeaux, France, 2014 (2014)
41. van Walraven, C., Musselman, R.: The surgical site infection risk score (SSIRS): a model to predict the risk of surgical site infections. PLoS ONE **8**(6), e67167 (2013). doi:10.1371/journal.pone.0067167. (Editor: Emma S. McBryde, Royal Melbourne Hospital)
42. Wiecek, M., Strkowski, R., Jakubowska, T., Wicek, B.: Software for classification of thermal imaging for medical applications (2016). https://www.researchgate.net/publication/237215535_Software_for_classification_of_thermal_imaging_for_medical_applications. Accessed 24 May 2016
43. Wilson, A.P., Treasure, T., Sturridge, M.F., Gruneberg, R.N.: A scoring method (ASEPSIS) for postoperative wound infections for use in clinical trials of antibiotic prophylaxis. Lancet **1**(8476), 311–313 (1986)
44. Zhou, Q., Li, Z., Aggarwal, J.K.: Boundary extraction in thermal images by edge map. In: ACM Symposium on Applied Computing SAC'04, Nicosia, Cyprus March 14–17 (2004)
45. Zhu, M., Ackerman, J.J.H., Sukstanskii, A.L., Yablonskiy, D.A.: How the body controls brain temperature: the temperature shielding effect of cerebral blood flow. J. Appl. Physiol. 101:1481–1488 (2006). First published Jul 13. doi:10.1152/japplphysiol.00319.2006